Thermal Distortion of Funnel Molds

Lance C. Hibbeler and Brian G. Thomas
University of Illinois at Urbana-Champaign
Department of Mechanical Science and Engineering
1206 West Green Street, MC-244
Urbana, Illinois, USA, 61802
Tel.: +1-217-333-6919
Fax: +1-217-244-6534
Email: lhibbel2@illinois.edu, bgthomas@illinois.edu

Ronald C. Schimmel[†] and Gert Abbel[‡]
Tata Steel
Strip Mainland Europe DSP[†], Research, Development, and Technology[‡]
P.O. Box 10,000
IJmuiden, The Netherlands, 1970 CA
Tel.: +31(0)251-492853[†], +31(0)251-492678[‡]
Email: ronald.schimmel@tatasteel.com, gert.abbel@tatasteel.com

Key words: Mold Distortion, Funnel Molds, Mold Wear, Narrow Face Taper, Computational Model

ABSTRACT

This paper investigates the thermal distortion of a funnel mold for continuous casting of thin slabs and explores the implications on taper and solidification of the steel shell. First, the three-dimensional mold temperatures are calculated using shell-mold heat flux and cooling water profiles that have been calibrated with plant measurements at Tata Steel IJmuiden. Next, the thermal stresses and distorted shape of the mold are calculated with a detailed finite-element model of a symmetric fourth of the entire mold and water box assembly, and are validated with plant measurements of the wear of the narrow face copper mold plates. The results of the simulations are evaluated for their influence on taper practice and water box design.

INTRODUCTION

The thermal distortion of the continuous casting mold from room temperature to steady operating temperatures can influence the behavior of the solidifying steel strand in many ways, but likely the most important of these is the narrow face taper practice. Mold distortion has been investigated by a few others in the past in billets[1,2], conventional thick slab molds[3,4], beam blank molds[5], and thin-slab funnel molds[6,7,8]. Owing to computer limitations in previous years, these models have not been able to contain all of the geometric details. These studies have revealed the importance of mold distortion on both mold taper, and cracks, and the importance of the waterbox on the mechanical behavior of the system. A complete quantitative analysis of funnel mold distortion, including realistic heat transfer, all of the important geometric details, proper constraints, shell/mold friction, and validation with plant measurements, has not yet been performed and is the aim of this study.

The main geometric features of the mold are shown in Figure 1. Other important details include, on the wide face, water channels 5 mm wide by 15 mm deep, cut with a ball end mill, set 25 mm from the hot face and at a 10 mm pitch. Each wide face has a rectangular array of 81 bolts at 125 mm pitch in the casting direction and 212.5 mm pitch in the perpendicular direction. The cooling channels next to each bolt hole are a pair of 10-mm diameter tubes. Each narrow face has one column of bolts at 134 mm pitch, and four cylindrical water channels of 14-mm diameter that are about 24 mm from the hot face. The geometry of the wide face water box is shown in Figure 2. The water box is built up from 20-, 30-, and 50-mm thick steel plates.

The remainder of this paper presents the numerical model used to investigate the distortion of funnel molds and then discusses in turn the thermal behavior, the mechanical behavior, the effect of distortion on taper practice, and validation with mold wear measurements.
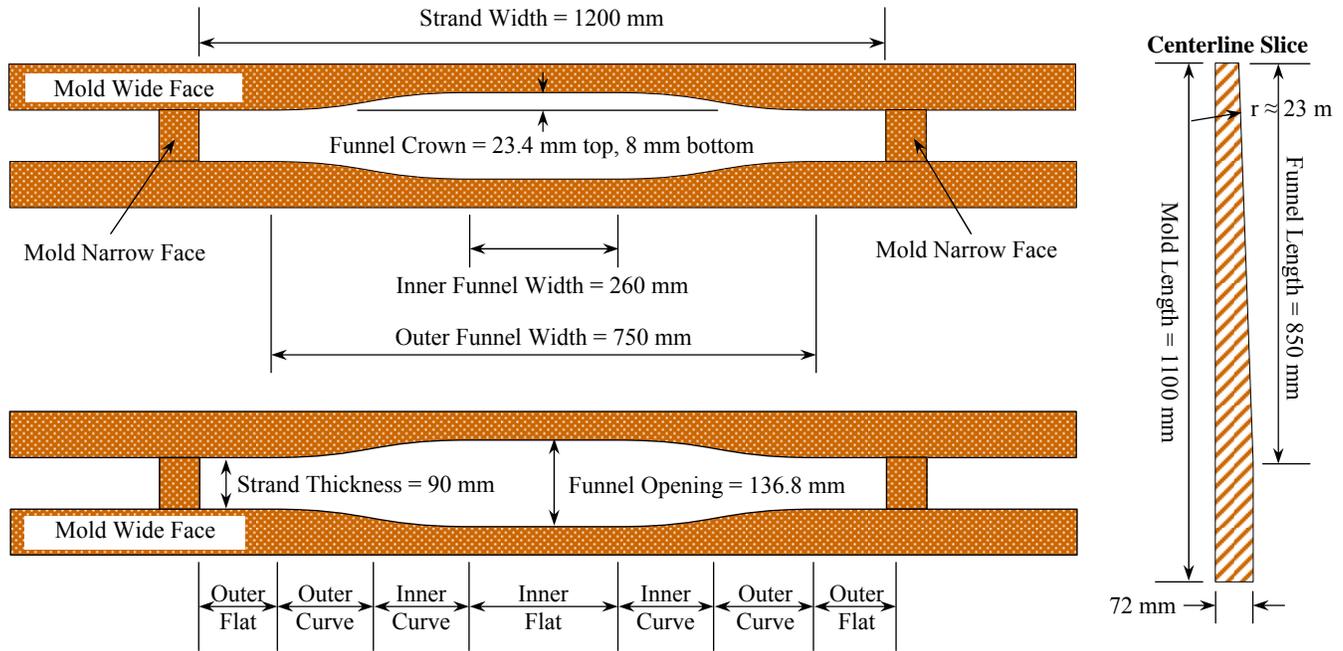
Fig. 1. Funnel Mold Geometry

Strand Width = 1200 mm

Mold Wide Face

Funnel Crown = 23.4 mm top, 8 mm bottom

Mold Narrow Face

Inner Funnel Width = 260 mm

Outer Funnel Width = 750 mm

Mold Narrow Face

Strand Thickness = 90 mm

Funnel Opening = 136.8 mm

Mold Wide Face

Outer Flat | Outer Curve | Inner Curve | Inner Flat | Inner Curve | Outer Curve | Outer Flat

Centerline Slice

$r \approx 23$ m

Mold Length = 1100 mm

Funnel Length = 850 mm

72 mm
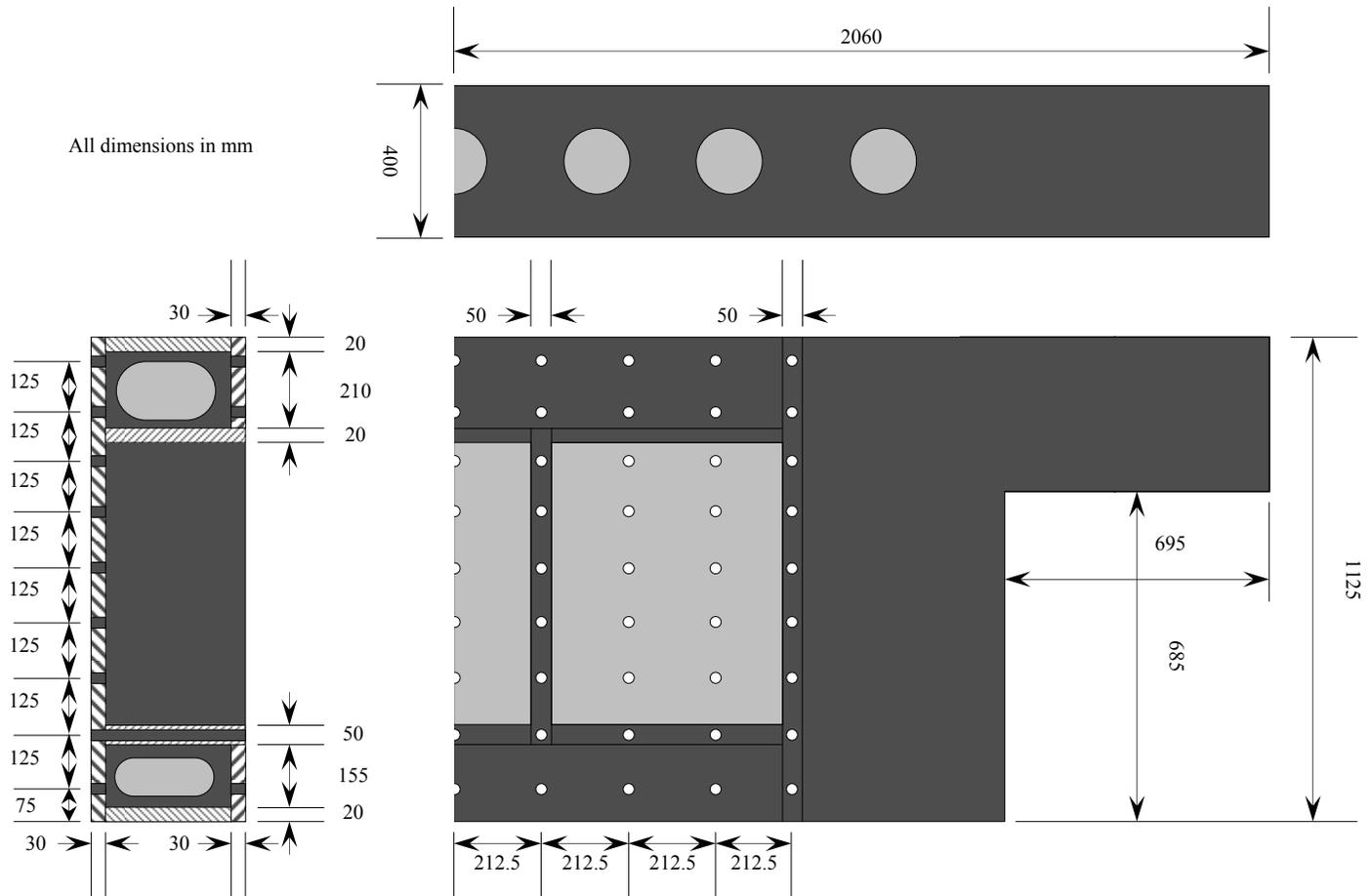
Fig. 2. Wide Face Water Box Geometry

2060

400

All dimensions in mm

30

125
125
125
125
125
125
125
125
125
75

20
210
20

50
155
20

30   30

50   50

212.5   212.5   212.5   212.5

695

685

1125

MODEL DESCRIPTION

The transport of thermal energy in a body is governed by the conservation of energy, and the response of a body to mechanical loading is governed by the equilibrium of forces. To investigate mold behavior during steady casting, the governing equations simplify considerably. The temperature distribution as a function of the three coordinate directions $T(x)$ is found by solving:

$$k \, \nabla^2 T = 0 \tag{1}$$

where k is the thermal conductivity. The mechanical behavior is governed by the differential equations of force equilibrium:

$$\nabla \cdot \boldsymbol{\sigma} = 0 \tag{2}$$

where $\boldsymbol{\sigma}(x)$ is the Cauchy stress tensor, computed from Hooke's law of linear elasticity:

$$\boldsymbol{\sigma} = \boldsymbol{C} : \boldsymbol{\varepsilon}^{el} \tag{3}$$

The fourth-order elastic stiffness tensor $\boldsymbol{C}$ is defined to be:

$$C_{ijk\ell} = \frac{E}{2(1+\nu)}\left(\delta_{ik}\delta_{j\ell} + \delta_{i\ell}\delta_{jk}\right) + \frac{\nu E}{(1+\nu)(1-2\nu)}\delta_{ij}\delta_{k\ell} \tag{4}$$

where E is Young's modulus, ν is Poisson's ratio, and δ_{ij} is the Kronecker delta (1 if $i = j$; 0 if $i \neq j$). The elastic strain tensor $\boldsymbol{\varepsilon}^{el}(x)$ is computed from an additive decomposition of the strains:

$$\boldsymbol{\varepsilon}^{el} = \boldsymbol{\varepsilon} - \boldsymbol{\varepsilon}^{th} \tag{5}$$

where $\boldsymbol{\varepsilon}(x)$ is the linearized total strain tensor, computed from the gradient of the displacement field $\boldsymbol{u}(x)$:

$$\boldsymbol{\varepsilon} = \tfrac{1}{2}\left(\nabla \boldsymbol{u} + (\nabla \boldsymbol{u})^T\right) \tag{6}$$

and $\boldsymbol{\varepsilon}^{th}(x)$ is the thermal strain tensor, calculated based on the coefficient of thermal expansion α and reference temperature T_0:

$$\boldsymbol{\varepsilon}^{th} = \alpha \left(T - T_0\right) \boldsymbol{I} \tag{7}$$

where $\boldsymbol{I} = \delta_{ij}$ is the second-order identity tensor. This strain decomposition does not include any inelastic effects, such as creep, since this study is not concerned with mold life issues.

The finite-element method was employed to solve the governing equations, using the commercial software ABAQUS[9]. A detailed representation of the mold plates and water boxes was constructed and discretized into many elements, as illustrated in Figure 1 with the details listed in Table 1. Although the water box is not perfectly symmetric, only one fourth of the entire mold and water box assembly was modeled in the interest of a feasible problem size. Most of the important geometric features were included in the model, including the funnel shape, the curved inlets and outlets of the water channels, thermocouple holes, and bolt holes. The entire mesh is shown in Figure 3. The mesh was refined around the more important geometric features, and the mold plates were meshed roughly four times more densely than the water boxes.

Table 1. Computational Model Mesh Details

Part	*Nodes*	*Elements*	
Wide Face Mold Plate	855,235	(Tetrahedra)	4,223,072
Wide Face Water Box	185,534	(Tet., Hexahedra, Wedge)	190,457
Wide Face Bolts	90	(Truss)	45
Tie Rods	4	(Truss)	2
Narrow Face Mold Plate	233,931	(Tet., Hex., Wedge)	495,566
Narrow Face Water Box	83,269	(Tet., Hex., Wedge)	239,604
Narrow Face Bolts	16	(Truss)	8
Total	1,358,079		5,148,754

For the thermal problem, the active areas of the hot face, extending below the meniscus from the centerlines to the edges where the narrow and wide face plates come into contact, were supplied a specified heat flux boundary condition:

$$-k \, \nabla T \cdot \boldsymbol{n} = \boldsymbol{q}^{sp} \cdot \boldsymbol{n} \tag{8}$$

where $\boldsymbol{q}^{sp}(x)$ is the specified heat flux vector and $\boldsymbol{n}(x)$ is the outward-pointing surface normal. The water channels were given convection heat flux boundary conditions:

$$-k \, \nabla T \cdot \boldsymbol{n} = h \left(T - T_\infty \right) \tag{9}$$

where $h(\boldsymbol{x})$ is the convection heat transfer coefficient and $T_\infty(\boldsymbol{x})$ is the sink temperature. The shell-mold heat flux, convection heat transfer coefficient, and cooling water temperature varied with position down the mold, as was calculated using the CON1D process model[10] and various plant data[11]. Figures 4, 5, and 6 show the values of these three thermal boundary conditions for the narrow face. The corresponding wide face values were only slightly different. These heat flux and convection data were input to ABAQUS via user subroutines DFLUX and FILM, respectively. The mold in this study has no coating layers, so the material properties were uniform throughout the entire mold and also were assumed constant with temperature. The thermal conductivity is given in Table 2. The water boxes were assumed to play no role in the thermal response of the mold, and were not included in the thermal analysis. The four mold parts together comprised 1,089,166 degrees of freedom, and this linear thermal problem required about 12 minutes to solve on a computer with an 8-core 2.66 GHz Intel Xeon processor and 8 GB of RAM.
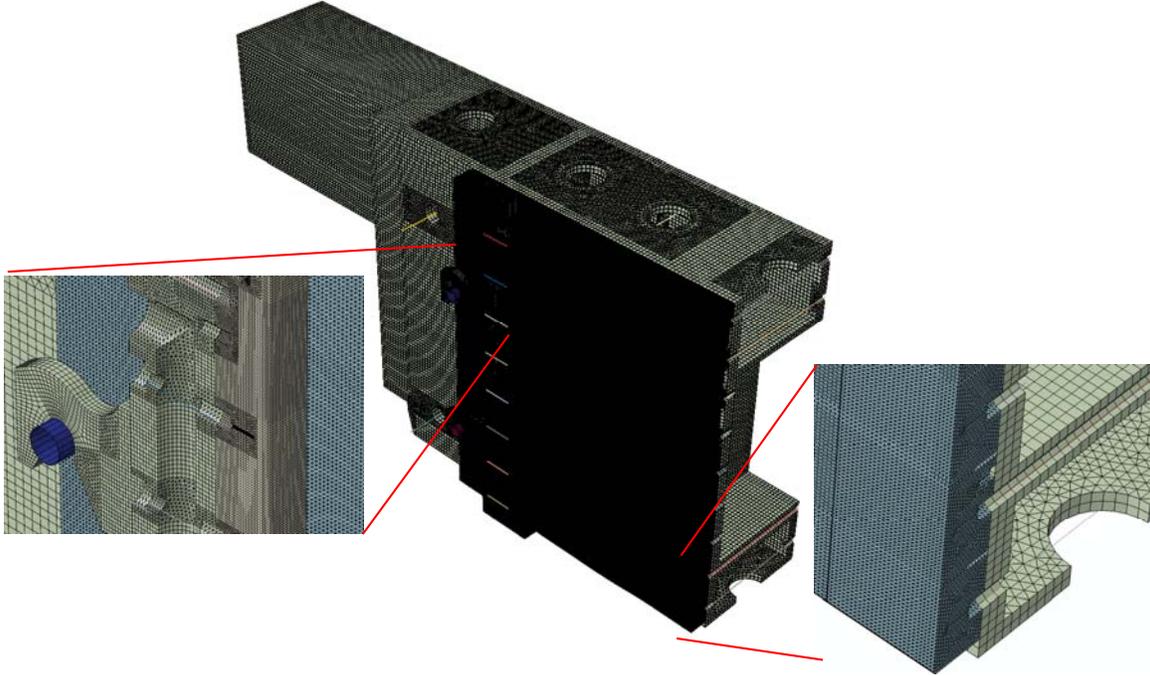
Fig. 3. Mold and Water Box Assembly Mesh
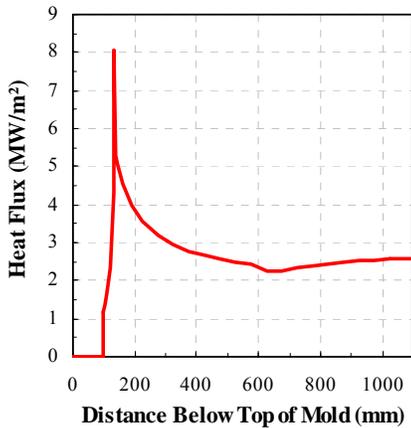
Fig. 4. Applied Heat Flux on Hot Face
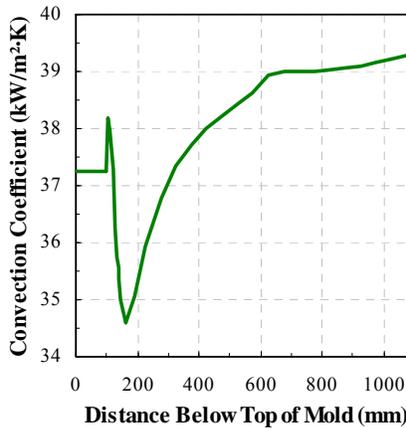
Fig. 5. Water Channel Convection Coefficient
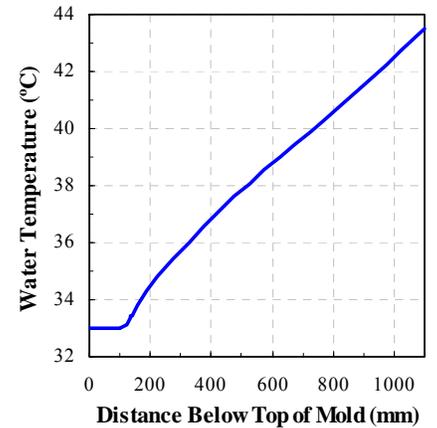
Fig. 6. Water Channel Water Temperature

The main driving force of the mechanical behavior of the mold is the thermal expansion, which was computed according to the temperature distribution calculated in the thermal model and Equation (6). The ferrostatic pressure was modeled as a distributed load that increased with distance below the meniscus according to the Bernoulli equation:

$$p = \rho \, g \, z \tag{10}$$

Table 2. Model Properties and Constants

Property or Constant	Value	
Mold material	Cu-Cr-Zr alloy	
Mold thermal conductivity, k_m	350	W/(m·K)
Mold Young's modulus, E_m	117	GPa
Mold Poisson's ratio, v_m	0.181	--
Mold coefficient of expansion, α_m	18	μm/(m·K)
Water box material	AISI 316Ti SS	
Water box Young's modulus, E_w	200	GPa
Water box Poisson's ratio, v_w	0.299	--
Mold-mold friction coefficient, μ_{mm}	1.0	--
Mold-waterbox friction coeff., μ_{mw}	0.5	--
Density of liquid steel, ρ	7100	kg/m³
Acceleration due to gravity, g	9.807	m/s²
Bolt friction, μ_b	0.3	--
Bolt thread pitch, λ	1.5	mm
Bolt tightening torque, τ	100	N·m

Table 3. Bolt Details

Bolt	Prestress (MPa)	Stiffness (MN/m)	Length Change (mm)
NF Short	168.51	240.0	0.12628
WF Short	162.00	424.4	0.07142
WF Long	211.5	62.76	0.4289
Top Tie Rod	32.91	133.47	1.1497
Bottom Tie Rod	57.60	133.47	2.094

where p is pressure, ρ is the density of the liquid steel, g is the acceleration due to gravity, and z is the distance below the meniscus. The pressure was applied only on the active areas of the hot face by utilizing the ABAQUS user subroutine DLOAD. The two cylinders that the narrow face hangs on were fixed in space, preventing rigid body motion in the narrow face. The large tie rods that hold the assembly together, the symmetry condition, and the friction between the narrow and wide faces prevent rigid body motion in the wide face. The mechanical contact between portions of the contacting surfaces of the two copper mold plates, and between each mold plate and its respective steel water box, was treated using the standard "hard" contact algorithms within ABAQUS with the static friction coefficients given in Table 2.

Each mold bolt was modeled as a truss element (extension degree-of-freedom only, ABAQUS element T3D2), and "distributing coupling constraints" (DCC) were used to connect the endpoint of this truss element to the appropriate element surfaces on the three-dimensional surface of the bolt hole, *i.e.*, the bolt threads and the mold outer surface contacting the bolt head, as illustrated in Figure 7. The DCC distributes the behavior of the truss element endpoint over the designated surface in an average sense such that the force and moment balances are maintained. Each simulated bolt was given a stiffness based on its length and the effective stiffness of the actual bolt. The bolts were prestressed according to plant practice. Details of the simulated bolts are presented in Table 2, including the length change due to the prestress. The bolt calculations performed here follow those done in previous work[3]. A density of 8900 kg/m³ for the mold copper gives weights of 0.5269 kN and 7.228 kN respectively for the narrow and wide faces. Uniformly distributing these over the appropriate number of bolts, the average shearing stress due to the mold weight is 0.3640 MPa and 0.5690 MPa. These are negligible relative to the prestress, so the effect of gravity was not needed in the numerical model. The mold assembly includes two tie rods that hold together the mold assembly. These were modeled in the same way as the mold bolts.
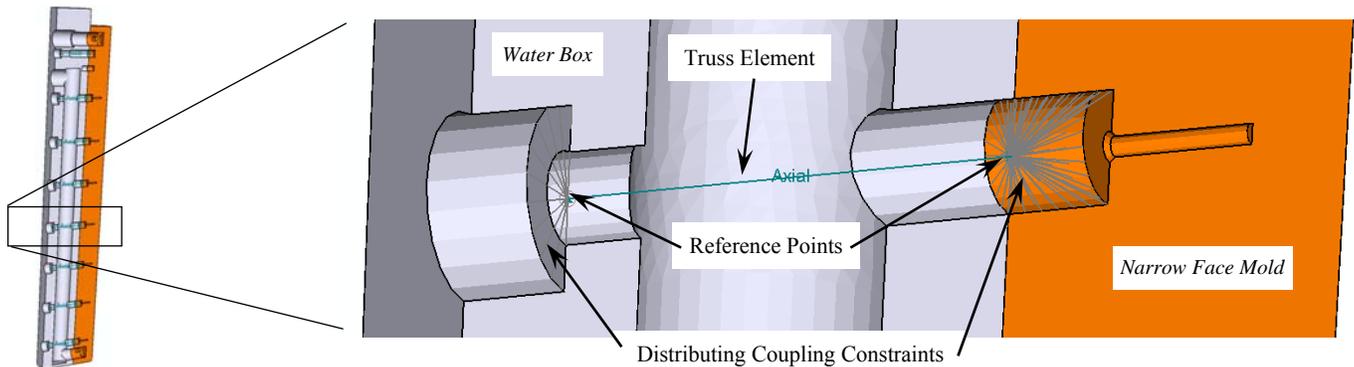
Fig. 7. Simulated Narrow Face Mold Bolt with Distributing Coupling Constraint

The mechanical model consisted of 4,830,081 degrees of freedom, and took 44.6 days to solve on a computer with an 8-core 2.66 GHz Intel Xeon processor and 8 GB of RAM. The large computational effort was required because of both the large problem size and the many iterations needed for the contact algorithms to converge. To assist in convergence of the nonlinear problem, the model was marched through pseudo-time, applying the thermal load as increasing strain percentages over ten steps.

MOLD HEAT TRANSFER

The calculated temperatures for the wide face mold are shown in Figures 8 and 9. The surface of the wide face shows variations in surface temperature around its perimeter mainly because of the variations in cooling channel design, *i.e.*, the vertical water tubes near the bolts do not extract heat as efficiently as the channels, leading to regions locally warmer by about 15 ºC. The mold also has a wide channel cut for the mold level sensor, but this effect is much smaller than the change in cooling around the bolt holes. The funnel

adds a slight two-dimensional effect to the heat extraction despite the water channels all being cut perpendicular to the back of the mold. The "inside-curve" region of the funnel extracts slightly more heat than the flat regions, resulting in a cooler shell and warmer mold. The outside-curve region of the funnel extracts slightly less heat, resulting in a warmer shell and a cooler mold. The funnel appears to have no other effect, owing to the consistent distance of the cooling channels from the hot face. The bottom portion of the mold shows higher surface temperatures by 60 to 120 ºC because the cooling channels cannot extend to the bottom of the mold. This effect is less near the water tubes because they extend further down the mold than the rectangular water channels.
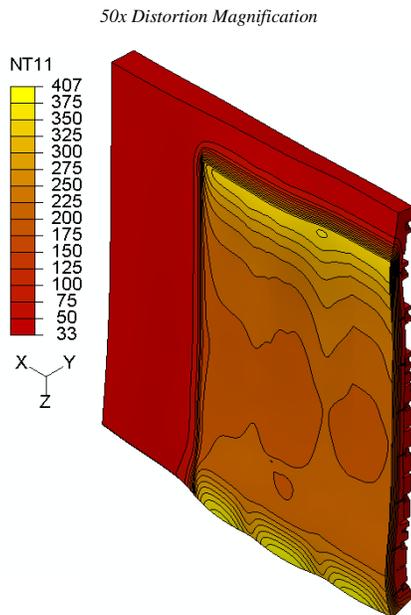
Fig. 8. Wide Face Temperature Contours (ºC)
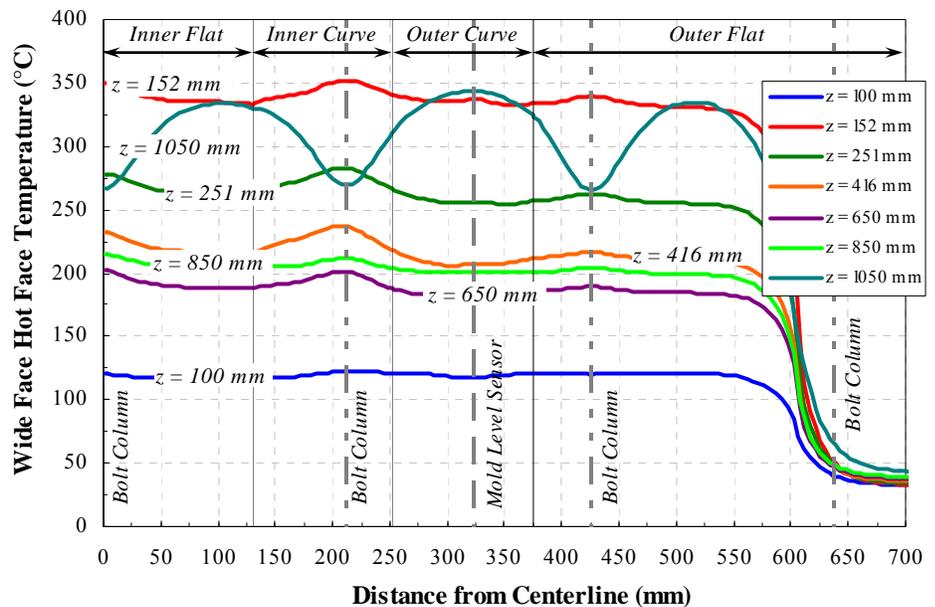
Fig. 9. Wide Face Temperature Profiles around the Perimeter

Temperature profiles around the mold perimeter are shown in Figure 9 at various distances down the length of the mold. The surface temperature of the mold is warmer locally by 10-25 ºC near the center of the inside curve region than surrounding areas, for most of the length of the mold. This higher mold temperature, and resulting change in heat transfer across the shell-mold gap, *may* help to cause longitudinal facial cracks (LFCs) in the shell. Previous work[12,13] identified that this region of the mold is prone to depression-style LFCs due to the bending in the shell caused by the funnel, and this variation in surface temperature may serve to exacerbate the problem.

The calculated temperatures for the narrow face mold are shown in Figures 10 and 11. The narrow face does not exhibit as much variation of surface temperature because the cooling channel design is more uniform. The mold hot face is curved slightly concave towards the molten steel to ensure that any bulging of the resulting convex-shaped strand during soft reduction below the mold is outward. The peak temperature in the center of the narrow face is 395 ºC. The extra copper between the water and the hot face serves to increase the mold hot face temperature slightly towards the slab corners.

MOLD DISTORTION

The primary focus of this study is the distortion behavior of the mold. The results in Figures 11-16 include displacement contours in the x- (NF) and y- (WF) directions, with larger values meaning distortion further away from the SEN. Figures 11-13 show the distorted shape of the narrow face mold copper plates and water box. Expansion of the copper hot face, constrained by the cold face and water box causes the entire assembly to bend into a parabolic arc, like a bimetallic strip. About 0.9 mm difference is predicted between the trough and tips of the arc. Distortion in the thin perimeter direction is very small. This classic behavior of the narrow face is expected and agrees with previous works[3,4]. The more interesting result on the narrow face is the fact that the generally parabolic distortion has a slight wobble in the middle of the mold, likely caused by the rigidity of the water-box hooks. This has important implications for the taper practice, as discussed later.

The distortion of the wide face mold and water box are shown in Figures 14-16. In general, the mold is pushed away from the molten steel by the ferrostatic pressure, but the thermal distortion causes it to bow towards the molten steel. This effect is most pronounced higher in the mold and in the middle of the outside curve region of the funnel. The peak of the bulge is coincidently found at the same point as the mold level sensor channel; the more relevant feature is that the peak occurs between two bolt columns. As shown in Table 3, the longer bolts have only about 15% the stiffness of the shorter bolts. Except for the top two and bottom two rows of bolts,

these longer bolts are attached to the mold through stiffener plates on the water box which offsets their lower stiffness in the bulk sense. Peaks in mold distortion in Figure 16 thus occur where the longer, more compliant bolts at the top and bottom two rows coincide with water-box cavities that lack extra stiffener plates. These cavities accommodate electromagnetic braking units, but also allow extra distortion. These peaks at 325 mm from the centerline at 200 and 1000 mm below mold top can also be seen in Figure 14. Regions near the middle of the mold with the shorter, stiffer bolts experience less distortion. Figures 17 and 18 show the temperature and distortion profiles down the wide face copper hot face at the centerline and middle of the outer curve region, where the distortion is most severe.
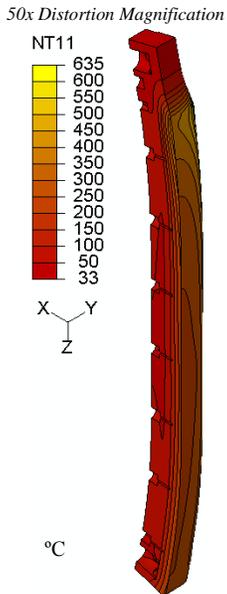
Fig. 10. NF Temperatures **Fig. 11. Narrow Face Centerline Temperature and Distortion** **Fig. 12. NF Water Box Dist.** **Fig. 13. NF Distortion**
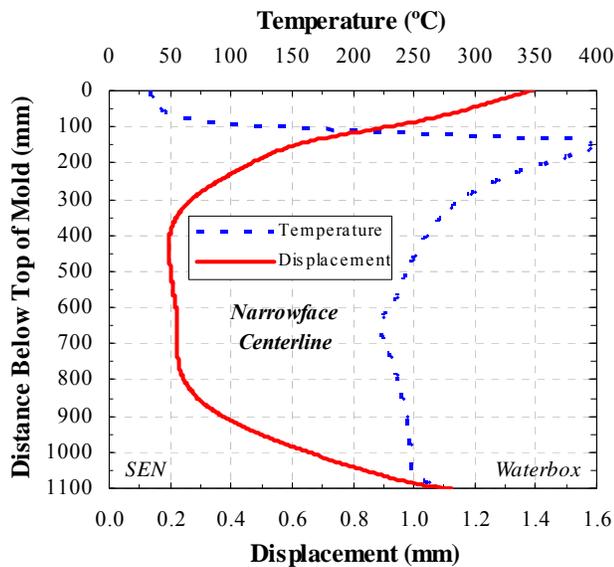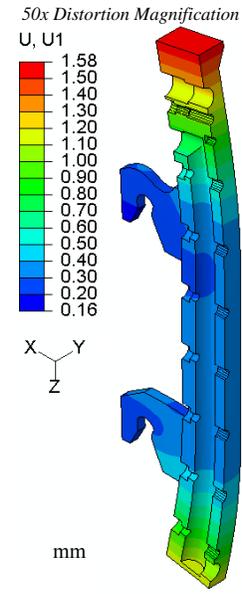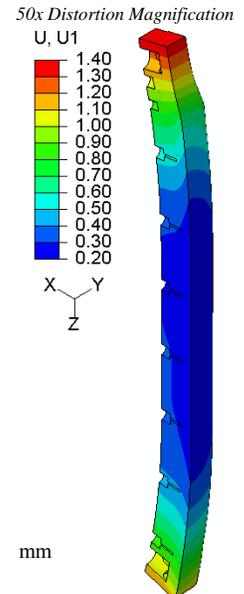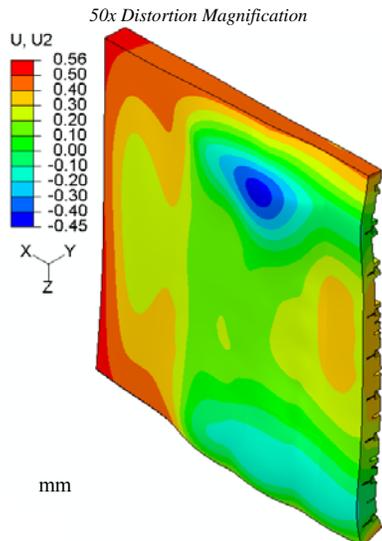
Fig. 14. Wide Face Mold Distortion **Fig. 15. Wide Face Water Box Distortion**
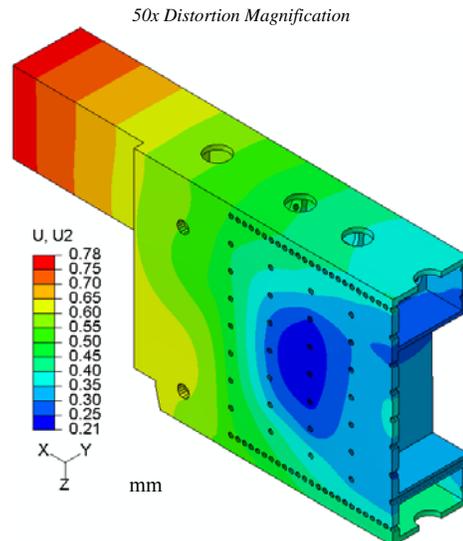
DISCUSSION AND PLANT EXPERIENCE

The mold distortion itself is not a problem, so long as it is understood and properly accounted for when constructing the mold and designing the narrow face taper practices. The narrow face experiences about 1 mm of distortion, which can greatly influence taper, since it is usually about 4-7 mm per narrow face. The wide face distorts about ±0.5 mm, which is less consequential because ferrostatic pressure can maintain contact of the large area of unsupported shell against the wide face. The more important aspect of the wide face distortion is the change in perimeter length caused by the distortion. Figure 19 quantifies this effect for the wide face by calculating the distorted perimeter length from the numerical model results and then subtracting off the perimeter length at the meniscus. This perimeter change is compared in Figure 19 with the perimeter change caused by the changing funnel shape on a cold mold. The line labeled Narrow Face is not the perimeter change of the narrow face, but is the distortion from Figure 11 that influences

the taper practice. The line labeled Total Distortion is the sum of the perimeter changes on the wide and narrow faces. This Total Distortion should be considered when designing narrow face taper of most clamped molds, where narrow face support is insufficient to prevent mechanical backlash and gaps from allowing the narrow face to move along with the wide face expansion.

Previous work[12,13] has investigated the shrinkage behavior of the solidifying shell in the funnel mold considered in this work, using a two-dimensional elastic-viscoplastic thermal-stress model. Figure 20 shows the predicted shell shrinkage at the narrow face from this previous work both with and without friction (0.16 static friction coefficient between the shell and mold). These predictions are also adjusted to include the effect of mold distortion that was calculated in this work. The commercial caster

Fig. 16. Wide Face Distortion Profiles around the Perimeter

uses 1%/m taper, which is 12 mm total for the 1200 mm strand width considered in this work. At room temperature, this is a straight line from the origin to 6 mm shrinkage at 1000 mm below meniscus in Figure 20. Clearly, the extra millimeter of perimeter length change significantly influences the mold shape relative to how the shell shrinks, and thus what taper should be applied on the narrow face. This point is explored further in Figure 21, which shows the difference between the lines in Figure 20 and the nominal 1%/m applied taper. In this figure, negative numbers mean the shell is shrinking more than the applied narrow face taper can accommodate, so a gap is opening between the shell and the mold on the narrow face. Positive numbers mean that the shell is pushing against the narrow-face mold wall, which would cause excessive mold wear, and other problems, such as off-corner buckling of the shell and longitudinal cracks. This figure shows that mold distortion and friction both greatly lessen the ideal narrow face taper needed to match the shell shrinkage. Neglecting either of these phenomena results in excessive taper, squeezing of the shell, and associated problems.
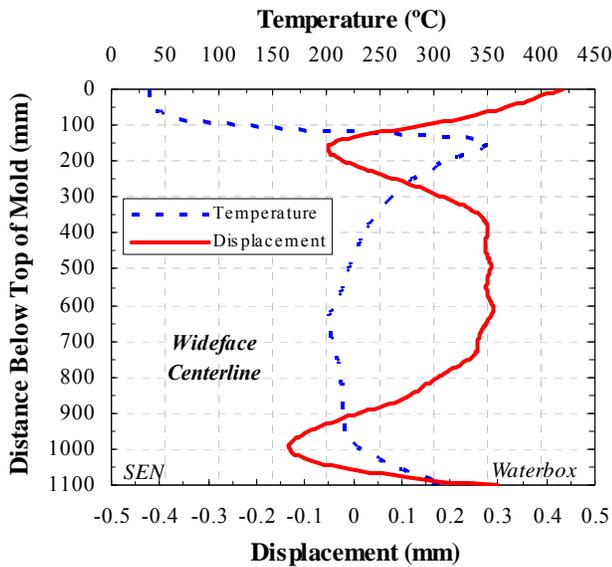
Fig. 17. WF Temperature and Displacement on Centerline
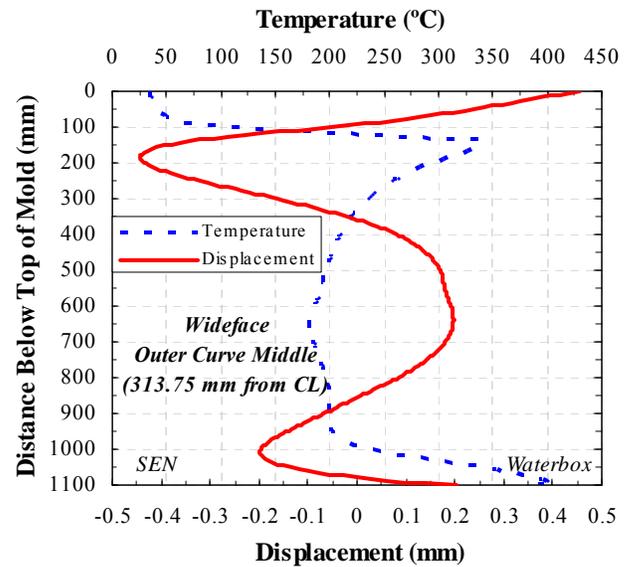
Fig. 18. WF Temperature and Displacement on Outer Curve Middle

Measurements of narrow face mold wear from the plant, shown in Figure 22, are consistent with the predictions in Figure 21. Minimum wear is observed between 200 and 500 mm below the meniscus. The higher wear towards the top and bottom of the mold agrees with the modeling prediction of two regions of positive numbers in Figure 21, caused by excessive taper. This problem can be treated in many ways: changing the bolt pattern, changing bolt tightness or grease, stiffening the water box, or changing the narrow face taper.
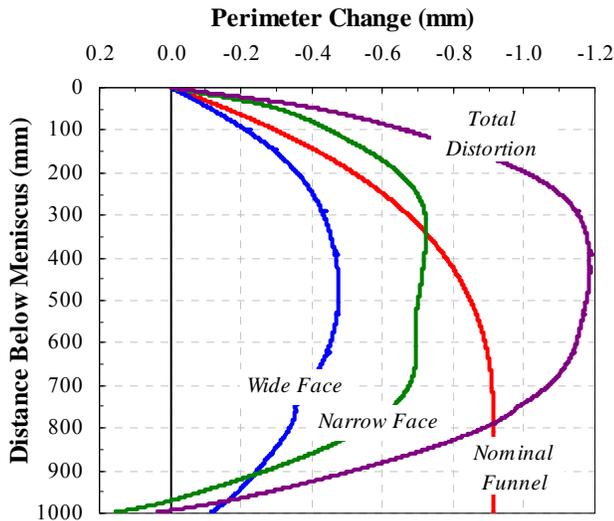
Fig. 19. Perimeter Change due to Mold Distortion
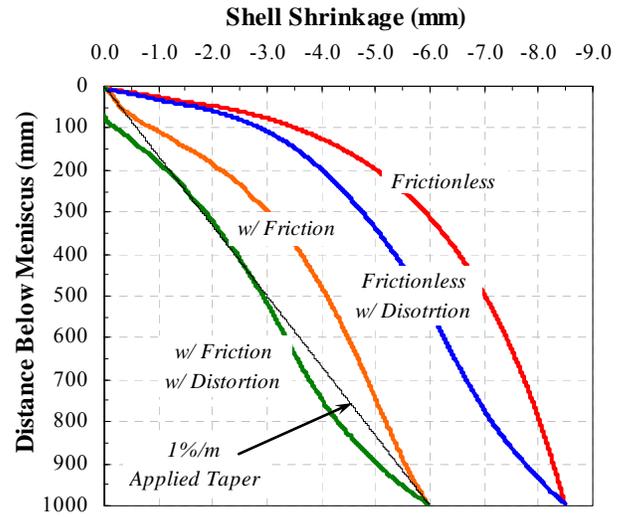
Fig. 20. Shell Shrinkage with Friction and Mold Distortion
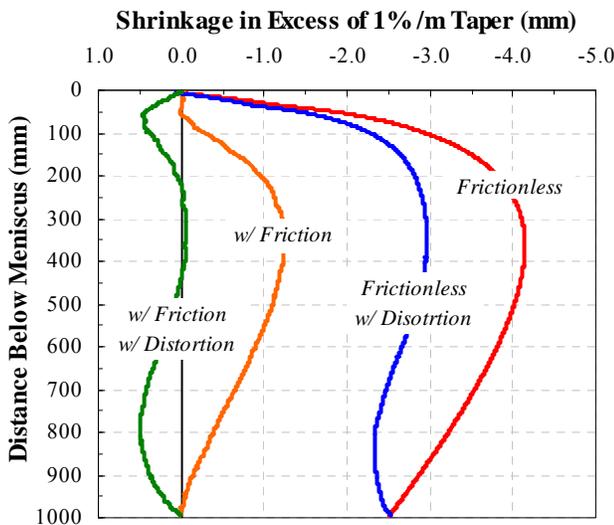
Fig. 21. Shrinkage Profiles with 1%/m NF Taper Removed
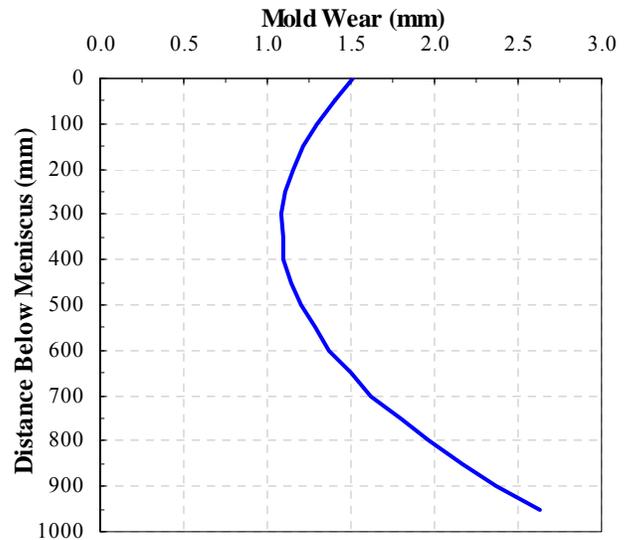
Fig. 22. Narrow Face Mold Wear Measurements

CONCLUSIONS

This paper provides insight into the thermal and mechanical behavior of a funnel mold continuous caster during steady casting, based on a nonlinear 3-D finite-element elastic stress analysis. The model features realistic thermal boundary conditions based on plant measurements from a previous study, complete geometric details of the slotted mold plates, tightened bolts, and water boxes, realistic contact, friction, and ferrostatic pressure. The thermal distortion of the narrow face is typical, bowing into a parabolic arch towards the molten steel. This accounts for about 0.7 mm of perimeter change of the wide face shell, and lessens the required narrow face taper. The wide face distorts into a complicated shape that depends on the bolt stiffnesses, and details of the water box construction. Wide face distortion accounts for about 0.4 mm of perimeter change. Combined with the mold distortion, this effectively increases the applied narrow face taper and can lead to regions of higher mold wear, as verified by measurements from the plant, or worse, shell buckling and cracks.

ACKNOWLEDGEMENTS

REFERENCES

1. I.V. Samarasekera and J.K. Brimacombe, "Thermal and Mechanical Behaviour of Continuous-Casting Billet Moulds." *Ironmaking and Steelmaking*, **9**:1 (1982), pg. 1-15.
2. Y. Hebi, Y. Man, Z. Huiying, and F. Dacheng, "3D Stress Model with Friction in and of Mould for Round Billet Continuous Casting." *ISIJ International*, **46**:4 (2006), pg. 546-552.
3. B.G. Thomas, G. Li, A. Moitra, and D. Habing, "Analysis of Thermal and Mechanical Behavior of Copper Molds During Continuous Casting of Steel Slabs." *Iron and Steelmaker*, **25**:11 (1998), pg. 125-143.
4. X. Liu and M. Zhu, "Finite Element Analysis of Thermal and Mechanical Behavior in a Slab Continuous Casting Mold." *ISIJ International*, **46**:11 (2006), pg. 1652-1659.
5. L.C. Hibbeler, K. Xu, B.G. Thomas, S. Koric, and C. Spangler, "Thermomechanical Modeling of Beam Blank Casting." *Iron and Steel Technology*, **6**:7 (2009), pg. 60-73.
6. T.G. O'Connor and J.A. Dantzig, "Modeling the Thin-Slab Continuous-Casting Mold." *Metallurgical and Materials Transactions*, **25B**:3 (1994), pg. 443-457.
7. J.K. Park, I.V. Samarasekera, B.G. Thomas, and U.S. Yoon, "Thermal and Mechanical Behavior of Copper Molds During Thin-Slab Casting (I): Plant Trial and Mathematical Modeling." *Metallurgical and Materials Transactions*, **33B**:3 (2002), pg. 425-436.
8. J.K. Park, I.V. Samarasekera, B.G. Thomas, and U.S. Yoon, "Thermal and Mechanical Behavior of Copper Molds During Thin-Slab Casting (II): Mold Crack Formation." *Metallurgical and Materials Transactions*, **33B**:3 (2002), pg. 437-449.
9. ABAQUS 6.9-1 User Manuals. 2009, Dassault Simulia, Inc., 166 Valley Street, Providence, RI, USA 02909-2499.
10. Y. Meng and B.G. Thomas, "Heat Transfer and Solidification Model of Continuous Slab Casting: CON1D." *Metallurgical and Materials Transactions*, **34B**:5 (2003), pg. 685-705.
11. B. Santillana, L.C. Hibbeler, B.G. Thomas, A. Hamoen, A. Kamperman, and W. van der Knoop, "Heat Transfer in Funnel-Mould Casting: Effect of Plate Thickness." *ISIJ International*, **48**:10 (2008), pg. 1380-1388.
12. L.C. Hibbeler, B.G. Thomas, B. Santillana, A. Hamoen, and A. Kamperman, "Longitudinal Face Crack Prediction with Thermo-Mechanical Models of Thin Slabs in Funnel Moulds." *La Metallurgia Italiana*, **6**:2 (2009), pg. 1-10.
13. L.C. Hibbeler, "Thermomechanical Behavior during Steel Continuous Casting in Funnel Molds." MS Thesis, The University of Illinois at Urbana-Champaign, (2009). Available at http://hdl.handle.net/2142/14636.